JOURNAL OF GUIDANCE, CONTROL, AND DYNAMICS
Vol. 25, No. 2, March–April 2002

Eccentricity Impact on East–West Stationkeeping for Global Positioning System Class Orbits

Todd A. Ely
Jet Propulsion Laboratory, California Institute of Technology, Pasadena, California 91109-8099

A strong relationship exists between eccentricity and the potential for an orbit that has a mean motion commensurate with the Earth's rotation rate to be chaotic. These complex motions can significantly impact the east–west stationkeeping (SK) process for maintaining the repeat groundtrack property of a commensurate orbit. Orbits with characteristics that are similar to the global positioning system (GPS) except that their eccentricities are modestly larger are investigated. It will be shown that at eccentricities greater than ~ 0.01 the chaotic regions become significant, and the need arises for a robust stable SK approach. Furthermore, an analytical model for eccentricity is developed, and the factors that contribute to its growth, thus increasing the probability of encountering chaotic motion during a typical satellite lifetime, are shown. These results are applied to selected GPS orbits. It is determined that, if the initial eccentricity is sufficiently large, then the traditional SK methods can destabilize and a more robust technique is required.

Introduction

THE extent to which an orbit with a mean motion commensurability to the Earth's rotation rate, that is, repeating groundtrack orbits, can be chaotic exhibits a strong relationship to the orbit's initial mean eccentricity.[1] This is true at all values of eccentricity, but perhaps most dramatic is that it is true even for orbits that are nearly circular. These complex motions can have a significant impact on the east–west stationkeeping (SK) process that maintains a commensurate orbit's repeating groundtrack property. The traditional SK method has been investigated thoroughly by many authors, including Gedeon,[2] Kamel et al.,[3] and Chao and Schmitt,[4] and is used extensively in many operational missions, including the global positioning system (GPS). The method targets maneuvers to graze specified stroboscopic mean node boundaries using simplifying assumptions about the nature of the dynamics in the phase space region near these boundaries. Ely and Howell[5] have shown that the traditional approach is unable to maintain a repeating groundtrack in the presence of complex dynamics, such as with chaotic dynamics. They developed an alternate SK method, called eccentric orbit SK (EOSK) that has proven successful at maintaing a repeating groundtrack for eccentric, commensurate orbits. In particular, eccentric orbits are more likely to encounter stroboscopic mean nodal accelerations (or an equivalent action rate) that pass through a value of zero and destabilize the traditional SK method. The EOSK approach has demonstrated its ability to remain convergent in the presence of these zeros.

The focus of the current study is to investigate satellite orbits with characteristics that are similar to those used by the GPS except that the selected eccentricities are modestly larger. It will be shown that at eccentricities greater than ~0.01 the chaotic regions become significant, and the need arises for a robust SK approach, such as the EOSK algorithm. Furthermore, the investigation reveals that the influence of luni–solar perturbations and tesseral perturbations (with a stationary stroboscopic mean node) contribute to the growth of eccentricity and, thus, increases the probability of encountering nodal accelerations that pass through a zero. Selected GPS orbits are examined and are found, given certain conditions on initial values, to need the EOSK algorithm to maintain track.

Formal Model Definition

A general long period dynamic model for the orbits considered in this study can be represented formally as an integrable Hamiltonian $H_0(I)$ being perturbed by additional conservative terms $\varepsilon H_1(I, \theta)$, where the variables (I, θ) represent action/angle variables.[6] The following is a brief summary of the relevant perturbations, a detailed development of the model may be found in Ref. 7. The Hamiltonian is transformed into a set of action/angle variables that prove convenient for studying mean motion resonances with the Earth.[1] Included in H_0 is the inverse square gravity term from a spherical Earth, a secular term due to the Earth's oblateness, that is, the potential energy term V^{ob}, and an additional term introduced because the reference frame is fixed in the Earth and rotates with it. The perturbation $\varepsilon H_1(I, \theta)$ includes long period potential energy terms from the Earth's tesseral harmonics (longitude dependent) V^t, the Earth's zonal harmonics (longitude independent) V^z, the moon's harmonics V^l, and the sun's harmonics V^s. Note, the superscript

Todd Ely received his B.S. and M.S. degrees in Aeronautical and Astronautical Engineering from Purdue University in 1986 and 1988, respectively. He served in the U.S. Air Force from 1988 to 1992, where he was assigned to the Milstar Joint Program Office and led a team of engineers to design, develop, and test an adaptive, autonomous orbit determination and control ground system that met Milstar's unique autonomy requirements. In 1992 he returned to Purdue to pursue a Ph.D., earning his degree in 1996 with his research on nonlinear resonance phenomena as applied to the long-term dynamics and control of satellite orbits. From 1997 to 1998 Ely held a Visiting Assistant Professor appointment at Purdue's School of Aeronautics and Astronautics, where he taught flight dynamics and controls systems analysis, and conducted research in the areas of satellite dynamics/controls and satellite constellation design. Currently, Ely is on staff at the Jet Propulsion Laboratory of the California Institute of Technology. He works on constellation design and navigation aspects of the Mars Network project, develops requirements for a new generation of mission design and navigation software, and conducts research in adaptive/autonomous deep space navigation. Ely is a senior member of the AIAA.

Presented as Paper AAS 99-389 at the AAS/AIAA Astrodynamics Specialist Conference, Girdwood, AK, August 1999; received 13 April 2000; revision received 31 August 2001; accepted for publication 1 September 2001.

ob is used when referring to Earth oblateness, t for tesseral terms, z for zonal terms, l for lunar quantities, and s for solar quantities. Formally, the Hamiltonian takes the following form:

$$H = H_0(I) + \varepsilon H_1(I, \theta) \tag{1}$$

$$H = -\frac{s_0^2\mu^2}{2I_1^2} - \dot{\theta}_e I_1 + V^{\text{ob}}(I_1, I_2, I_3) + \sum V^t(I_1, I_2, I_3, \lambda, \omega) + \sum V^z(I_1, I_2, I_3, \omega) + \sum V^l(I_1, I_2, I_3, \omega, \Omega, \Omega_l) + \sum V^s(I_1, I_2, I_3, \omega, \Omega, \Omega_s) \tag{2}$$

where the action/angle pairs are defined as follows:

$$I_1 = s_0 L = s_0\sqrt{\mu a}, \qquad \lambda = (1/s_0)(M + \omega) - (\theta_e - \Omega)$$
$$I_2 = L\sqrt{1 - e^2} - L, \qquad \omega$$
$$I_3 = L\sqrt{1 - e^2}\cos i - s_0 L, \qquad \Omega \tag{3}$$

The variables a, e, i, M, ω, and Ω represent the classical elements defining the mean orbit associated with a given trajectory. Additionally, s_0 is the integer nearest the ratio of satellite mean motion over Earth rotation rate, that is, $s_0 = 2$ is associated with a 12-h orbit, μ is the product of the gravitational constant and the Earth's mass, θ_e is the Greenwich sidereal angle, and $\dot{\theta}_e$ is its associated rate. The quantity Ω_l is the longitude of the ascending node of the lunar orbit (referenced to the ecliptic plane), and Ω_s is the ascending node of apparent solar orbit (referenced to the equatorial plane). Note that the angle λ, called the stroboscopic mean node, has a slow variation in time due to the commensurability between satellite mean motion and the Earth's rotation rate, that is, $(\dot{M} + \dot{\omega})/s_0 + \dot{\Omega} \approx \dot{\theta}_e$. Furthermore, the argument of perigee ω and the right ascension of the ascending node Ω vary slowly, primarily because of Earth's oblateness. The ascending nodes Ω_l and Ω_s vary linearly with time.

SK Performance as a Function of Eccentricity

A Poincaré section is a useful tool for analyzing the relationship between eccentricity and the chaotic regions of phase space produced by an eccentric, commensurate orbit. Figure 1 shows two plots: Fig. 1a is a Poincaré section of orbits with initial values of $\{a, e, i, \Omega, \omega, M\} = \{$various values within $26{,}560 \pm 5$ km, 0.01, 55 deg, 0 deg, 65 deg, -47 deg$\}$; Fig. 1b is similar except the initial eccentricity has been increased to 0.02. The dynamic model used to produce the trajectories is long period with secular oblateness effects and critical tesseral harmonics up to fourth order and degree (no other zonal and luni–solar perturbations are present). Note the existence of chaotic regions in both plots (identified by the scattered dots) and the marked increase in the complexity and extent of these regions in the plot with $e = 0.02$ as compared to $e = 0.01$. Previous research has shown that the implication of these complex dynamics is that the traditional east–west SK method is much more likely to become unstable, that is, the action rate $\dot{I}_1$, or, equivalently, the nodal acceleration $\ddot{\lambda}$, changes sign during an SK cycle, in these regimes.[5] To assess this possibility, it is instructive to analyze the equations of motion associated with a satellite that is controlling its stroboscopic mean node so that it remains within a specified deadband region, that is, east–west SK,

$$\dot{I} = \sum_{q=0} m h^t_{lmpq}(a^*, e^*, i^*)\sin[m(\lambda - \lambda_{lm})] + \sum_{q\neq 0} m h^t_{lmpq}(a^*, e^*, i^*)\sin[m(\lambda - \lambda_{lm}) - q\omega(t)] \tag{4a}$$

$$\dot{\lambda} = -\frac{3}{s_0^2 a^{*2}} I \tag{4b}$$

$$\dot{\omega} \equiv \dot{\omega}_{\text{sec}} = \frac{\partial H_0}{\partial I_2^*} = \frac{3}{2}\frac{J_2 n^*}{\left(1 - e^{*2}\right)^2}\left(\frac{R_e}{a^*}\right)^2\left(2 - \frac{5}{2}\sin^2 i^*\right) \tag{4c}$$

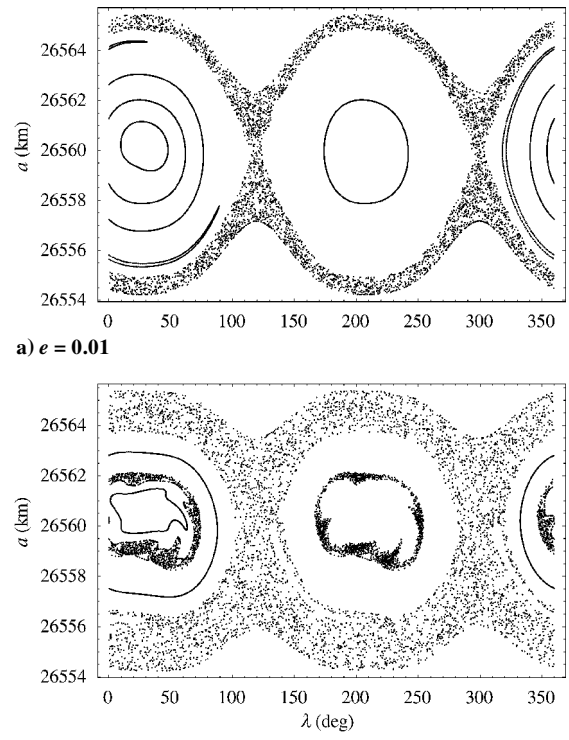

Fig. 1 Poincaré section of GPS class of orbits for different eccentricities, $\omega = 65$ deg.

Equation (4) represents a local dynamic model that is reduced from Eq. (1); the reduction procedure can be found in Ref. 5. It has $\frac{3}{2}$ degrees of freedom with phase variables that include the action $I \equiv I_1 - I_1^* = s_0(L - L^*) \approx s_0\sqrt{(\mu/a^*)}(a - a^*)/2$, the stroboscopic mean node λ, and perigee ω. Parameters with asterisks represent values of the associated variable at the location of the exact commensurability between the secular rates, that is, $\dot{\lambda} = 0$. Proceeding in a manner similar to the classical control strategy, the node in Eq. (4a) is fixed to a specified nominal value λ_n. It is around this nominal value that the SK process controls the orbit to remain inside of a specified deadband region $\Delta\lambda$. Within the deadband, the node is allowed to drift. SK maneuvers are performed when the orbit drifts to a boundary of the deadband.

Utilization of this control strategy changes the nature of the dynamic response due to the perturbing tesseral harmonics [$h^t_{\text{lmpq}}(\cdot)\sin(\cdot)$ in Eq. (4a)]. Indeed, the chaotic response is eliminated; however, the tesserals still produce dynamic artifacts of interest. Because λ is nearly stationary, the terms with $q = 0$ can be considered constant. However, the terms with $q \neq 0$ are nonautonomous because of their dependence on perigee (a time-varying quantity). This functional dependence on time invalidates two fundamental assumptions in the classical SK method: The nodal time history is not symmetric around the exact resonance value, and the nodal acceleration is not guaranteed to have a constant sign within a cycle (or, equivalently, the action rate can pass through a value of zero).

To determine regions of phase space that have the potential to encounter a passage through an action rate zero, set Eq. (4a) equal to zero. The result yields a function of node λ and perigee ω that is parameterized by eccentricity when the semimajor axis is set to the exact resonance value a^* and the inclination is specified. In the case of a GPS orbit, the resonant semimajor axis takes a value of 26,560 km, that is, a 12-h orbit, and the inclination is set to 55 deg. Figure 2 shows the location of the action rate zeros for selected values of eccentricity. Note that the behavior of these locations becomes increasingly complex with a modest growth in eccentricity. At an inclination of 55 deg, perigee varies in a nearly secular fashion and, for a mission lifetime of 10 years, can be expected to change by $\sim$100 deg. Hence, if a satellite initial condition is placed near a line of zeros with an irregular shape, then there exists an increased

possibility of encountering the zero as perigee evolves. This possibility also becomes greater with an increase in initial eccentricity.

Two examples are considered using elements selected from the GPS constellation, but with eccentricities that are modified slightly from the ideal circular case. Some of the mean elements that are common to all of the satellites in the GPS constellation include semimajor axis and the inclination, which take the values defined earlier. The elements that are unique for each satellite in the constellation include the ascending node Ω and the argument of latitude ($u = \omega + M$). These elements are carefully selected so that the GPS constellation can achieve its required coverage objectives, that is, four satellites in view by any ground station at all times. On the other hand, specifications for eccentricity and perigee are secondary. Optimally, eccentricity should be zero, and as a result, perigee would be undefined. However, this idealized situation can never be realized in practice. The actual orbits always posses small eccentricity and, thus, a value for perigee. Indeed, the GPS program has a requirement to inject their satellites into final drift orbits with eccentricities no greater than 0.012. Thus, it is entirely possible that a particular combination of elements could yield a situation where the node will encounter a zero. Table 1 lists those satellites in the planned GPS constellation that have values of the stroboscopic mean node nearest the action rate zero locations, as shown in Fig. 2. These orbits have the most potential to encounter SK instabilities in their lifetimes. Note that the epoch associated with the elements is 15 April 1999, which yields a mean Earth sidereal angle of $\theta_e = 202.71$ deg. The two cases studied are associated with satellite A4. In the first case, the initial eccentricity has a value of 0.01, and in the second, it is initially 0.02. In both cases, perigee has been set to zero. The selected deadband region has a width of 4 deg and a nominal nodal value of $\lambda_n = 14.698$ deg. The boxes shown in Fig. 2 for $e = 0.01$ and 0.02 have sides with lengths equal to the deadband and a 100-deg change in perigee, that is, a 10-year mission. The boxes indicate the possibility of encountering an action rate zero during the lifetime of a mission. Examination of Fig. 2 shows that the selected initial conditions are such that the first case, with $e = 0.01$, does not encounter a zero over the satellite lifetime, and the second case, with $e = 0.02$, does.

Both cases utilize the EOSK algorithm developed in Ref. 5 for use with orbits that encounter action rate zeros. The controlled orbits are simulated for several thousand days with the results for the semimajor axis, eccentricity, and node shown in Figs. 3 and 4. Additionally for the second case, the traditional SK algorithm is simulated to illustrate its inability to maintain the node within the designated deadband of (12.7, 16.7 deg). The force model used in the propagation includes tesseral, zonal, and luni–solar effects. As expected for the first case, shown in Fig. 3, the trajectory does not encounter an action rate equal to zero, and the nodal history exhibits the traditional scallop shape. In the second case, the solid lines in Fig. 4 represent results of the EOSK algorithm, and the dashed lines represent results from the traditional SK algorithm. As expected, the trajectory passes through an action rate equal to zero. Evidence of this can be seen in the irregular nodal history from the

Table 1 GPS satellite locations nearest action rate zeros

Satellite	Ω, deg	$u = \omega + M$, deg	λ, deg
A4	188.089	58.638	14.698
E2	68.089	319.428	25.093
C2	308.089	28.628	119.693
B3	248.089	326.808	208.783

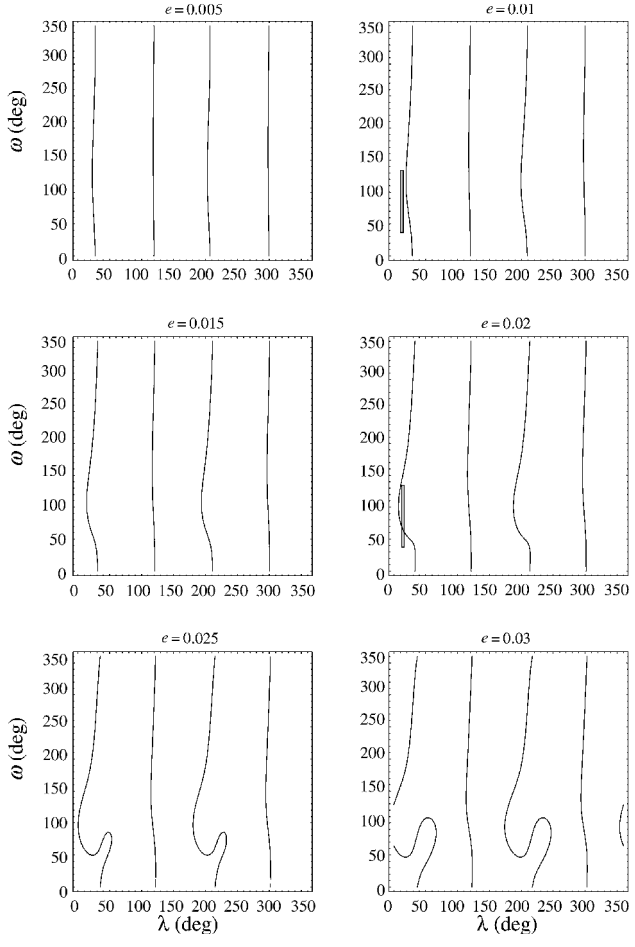

Fig. 2 Action rate zeros parameterized by eccentricity.

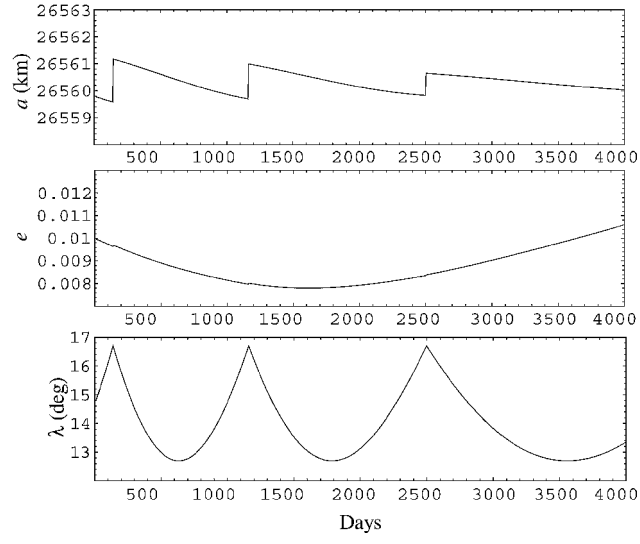

Fig. 3 SK cycle for the case with $e = 0.01$; no action rate zeros encountered.

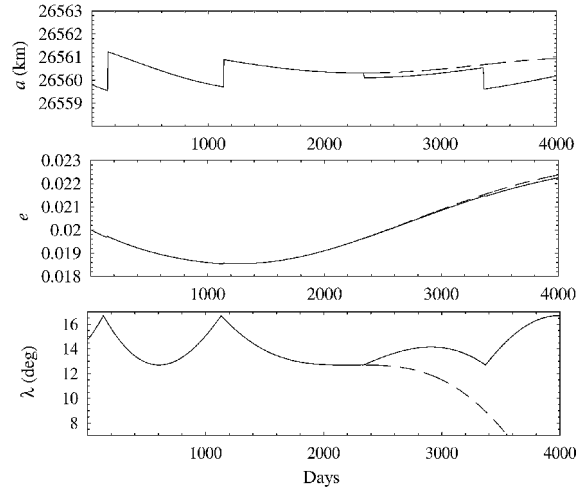

Fig. 4 SK cycle for the case with $e = 0.02$; action rate zero encountered in the third cycle (1100–2400 days) and the EOSK algorithm (——) compensates for the zero.

EOSK algorithm (solid line) of Fig. 4 during the second cycle from 1100 to 2400 days. This is typical of the algorithm as it changes its grazing and burn boundaries to accommodate the sign change in the nodal acceleration. The EOSK algorithm is successful at keeping the node within the desired deadband region during the entire mission. The traditional algorithm results (dashed line) show the failure of the algorithm at keeping the nodal history within the designated deadband; the node traverses the lower boundary at 12.7 deg near 2200 days into the simulation. Note that in the first case, the eccentricity variation was approximately $\Delta e \sim 0.003$, and in the second case the variation was ~0.004. Clearly, a different value for initial perigee or epoch coupled with a shift in eccentricity could bring the orbit into a regime where an action rate zero can occur during the mission lifetime. A better understanding of the behavior of eccentricity is desirable so that the SK instability issue can be assessed more thoroughly.

Long-Term Eccentricity Behavior

The preceding discussion illustrated the central role that eccentricity has in determining the possibility of an encounter with an action rate zero. Thus, it would be beneficial to develop an analytical representation for the behavior of eccentricity as a function of time. Much has been published in this area, and it is conventional wisdom that luni–solar perturbations can have a significant impact on the behavior of eccentricity. Giacaglia[8] has written a thorough review of nearly 40 years of published results regarding the effects of luni–solar perturbations on artificial satellite orbits. However, most previous work has not dealt with the issue of lunar resonance overlap and its consequences on long-term eccentricity behavior. Ely and Howell[7] have shown that there exists an intricate web of luni–solar resonances that can interact to produce chaotic and diffusive motion. The locations of the significant resonances can be located by analyzing linear combinations of the form $m_1\dot{\omega} + m_2\dot{\Omega} + m_3\dot{\Omega}_l \approx 0$ or $m_1\dot{\omega} + m_2(\dot{\Omega} - \dot{\Omega}_s) \approx 0$, where (m_1, m_2, m_3) represent a vector of integer numbers that identify particular harmonic terms (and, thus, resonant terms) in the perturbation expansion. The resonance interactions have dominant effects on the extremely long-term behaviors of $\{e, i, \omega, \Omega\}$. Even though the timescales for such motions are typically much longer than that of a satellite mission, it is instructive to understand the nature of the global dynamics and the timescales necessary to observe these dynamics. With this information, it is possible to assess the timescales that an asymptotic theory will be valid. That is, a first-order averaging approach yields a solution that is accurate to $\mathcal{O}(\varepsilon)$ on a timescale of order $\mathcal{O}(1/\varepsilon)$. An analysis of the potential for chaos and/or diffusion allows for a quantitative assessment of this timescale.

To illustrate the phenomena, a selected GPS-like initial condition, $(a, e, i, \omega, \Omega, M) = (26{,}560$ km, 0.02, 55 deg, 0 deg, 8 deg, 52 deg), is propagated for approximately 60,000 years. The dynamic model used consists of only long-period luni–solar perturbations (geopotential terms other than secular oblateness are not present). This yields a set of dynamic equations that are not stiff and, hence, amenable to such a long-term propagation. To illustrate the behavior of the motion, the inclination and eccentricity are sampled on returns to a specified ascending node value (arbitrarily selected to be 100 deg) and are plotted as a point on the inclination/eccentricity plane. The time span between consecutive points is approximately 20 years. The results are shown in Fig. 5 as an array of plots. Each plot is a snap shot in time. The upper left plot represents the first 500 samples (~9950 years), and the lower left includes all 3000 samples (~59,692 years). Also shown in Fig. 5 are the locations of the significant luni–solar resonances, that is, $m_1\dot{\omega} + m_2\dot{\Omega} + m_3\dot{\Omega}_l \approx 0$ or $m_1\dot{\omega} + m_2(\dot{\Omega} - \dot{\Omega}_s) \approx 0$, as functions of inclination and eccentricity. They appear as the complex web of intersecting lines. The initial condition is indicated and is located near the dominant luni–solar resonances that impact the GPS constellation. Specifically, the largest nearby resonance is associated with luni–solar harmonic terms that have an angular argument of $(2\omega + \Omega)$. The straight line at the 56-deg inclination (at all eccentricities) identifies the resonance location. The other resonance is associated with a lunar harmonic with angular argument of $(2\omega + \Omega_l - \pi)$. This produces the curved line beginning at approximately 53.3-deg inclination. Clearly, for

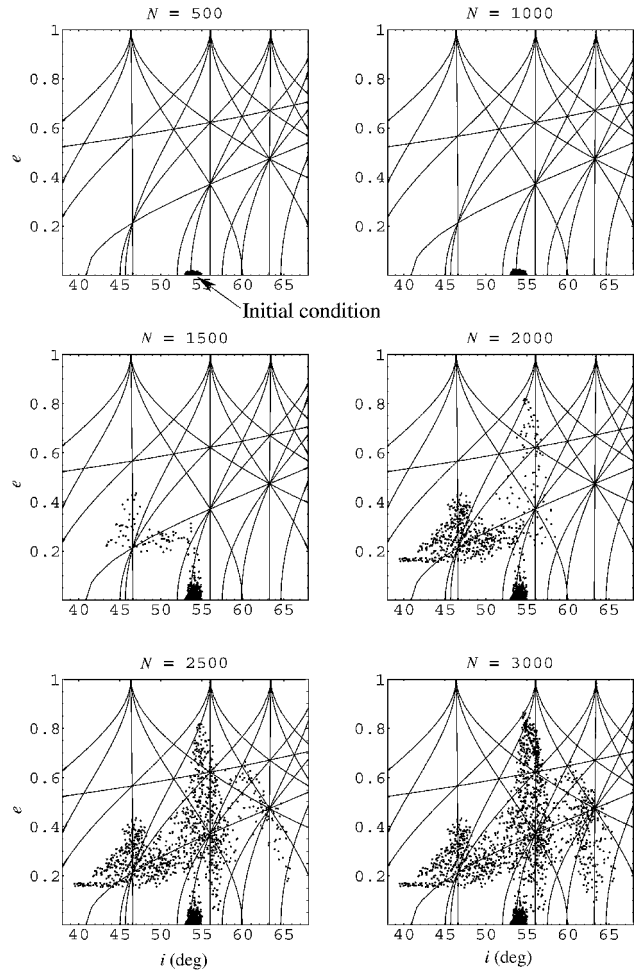

Fig. 5 Extremely long-term behavior of eccentricity vs inclination for a GPS-like orbit; dynamics illustrate chaos and diffusion as it follows resonance locations.

the first 1000 points the trajectory remains confined to the region of these two resonances. The behavior is actually chaotic; however, the motion does not exhibit any large-scale excursions in eccentricity or inclination. Then, between 1000 and 1500 samples, the trajectory experiences large-scale diffusion. As is typical of this type of motion, there exists a tendency for the trajectory to follow a resonance curve, and then, at an intersection with another resonance, it jumps to follow the other curve. The example also illustrates the potential for an initially near circular orbit to become nearly hyperbolic under the influence of only luni–solar perturbations.

Analytical Eccentricity Model

Because mission timescales, which are on order of 10–15 years, are much shorter than the time frames shown in Fig. 5, it is reasonable to expect an asymptotic theory to produce qualitatively accurate eccentricity histories for the span being considered. Indeed, results will show that the analytical model developed in this study compares favorably with numerically generated results. Specifically, the behavior of eccentricity in the region of a GPS orbit is of interest; therefore, the model includes only those perturbations that dominate near an inclination of 55 deg and for eccentricities near zero. The impact of individual harmonic terms is assessed by analyzing the magnitude of their coefficients divided by the secular rate of their angular argument, that is, the magnitude of the harmonic coefficients of the analytically integrated solution. Those with the largest coefficients are retained. Also, note that, for the timescale of interest, the orbit is only in shallow resonance with harmonic terms of the form $h(a, e, i)\cos(2\omega + \Omega)$. It is sufficiently shallow that a standard perturbation method can be utilized to integrate the equation of motion that includes these terms. The other resonance terms have insufficient time to impact significantly the motion and,

hence, can be neglected. As the earlier discussion indicated, if the timescale were longer, then these assumptions would not be valid.

The other key feature affecting the behavior of eccentricity is associated with the tesseral harmonics. Controlling the stroboscopic mean node to be nearly stationary introduces a coupling between eccentricity and the tesseral harmonics that would not ordinarily exist because the timescale of the nodal advance is much faster than that of perigee. However, because the controlled nodal rate is effectively zero, the angular rate associated with some of the tesseral harmonics can now be attributed primarily to the perigee rate. With the preceding observations in mind, a Hamiltonian of long-period terms can be formulated that is specialized for the phase space region applicable to the class of orbits that are near circular and at an inclination near 55 deg. It is written formally as

$$\begin{aligned} H_{\mathrm{GPS}} &= V^{\mathrm{SEC}}_{\mathrm{GPS}} + V^{l}_{\mathrm{GPS}} + V^{s}_{\mathrm{GPS}} + V^{t}_{\mathrm{GPS}} + V^{z}_{\mathrm{GPS}} \\ &= V^{\mathrm{SEC}}_{\mathrm{GPS}} + \left(h^{l}_{2\omega} + h^{s}_{2\omega}\right)\cos 2\omega + h^{l}_{2\omega+\Omega}\cos(2\omega+\Omega) \\ &\quad + h^{s}_{2\omega+\Omega-\Omega_s}\cos(2\omega+\Omega-\Omega_s) + h^{t}_{2(\lambda-\lambda_{32})}\cos[2(\lambda-\lambda_{32})] \\ &\quad + h^{t}_{2(\lambda-\lambda_{22})+\omega}\cos[2(\lambda-\lambda_{22})+\omega] + h^{t}_{2(\lambda-\lambda_{22})-\omega} \\ &\quad \times \cos[2(\lambda-\lambda_{22})-\omega] + h^{z}_{\pi/2-\omega}\cos(\pi/2-\omega) \end{aligned} \tag{5}$$

where the secular term includes Earth's oblateness and luni–solar contributions. This term yields the secular rates for perigee $\dot{\omega}_{\mathrm{sec}}$ and the ascending node $\dot{\Omega}_{\mathrm{sec}}$. The detailed equations for these rates and the long-period harmonic terms in Eq. (5) are found in the Appendix. Note that the lunar orbital parameters are referenced to the ecliptic plane, and all others (including the solar parameters) are referenced to the Earth's equatorial plane. For purposes of the analytical model, the node λ and solar ascending node Ω_s are held constant. The equation of motion for eccentricity is obtained by applying the following perturbation equation to Eq. (5):

$$\begin{aligned} \frac{\mathrm{d}e}{\mathrm{d}t} &= \frac{\sqrt{1-e^2}\left(1-\sqrt{1-e^2}\right)}{s_0 n a^2 e}\frac{\partial H}{\partial \lambda} + \frac{\sqrt{1-e^2}}{na^2 e}\frac{\partial H}{\partial \omega} \\ &\approx \frac{e}{2s_0 n a^2}\frac{\partial H}{\partial \lambda} + \frac{1}{na^2 e}\frac{\partial H}{\partial \omega} \end{aligned} \tag{6}$$

Proceeding in the standard way, the equation of motion can be analytically integrated by holding the harmonic coefficients constant and using the secular rates to evaluate the angles as linear functions of time. The result is an equation for eccentricity that is a function of time and the initial mean elements, and, formally, takes the form

$$\begin{aligned} e(t) &= e_0 + \sum_{\{(m_1,m_2,m_3,m_4,m_5)\}} \frac{C(a_0, e_0, i_0; \text{parameters})}{m_1\dot{\omega} + m_2\dot{\Omega}} \\ &\quad \times \left\{ \cos\left[m_1\omega(t) + m_2\Omega(t) + m_3\lambda_n + m_4\Omega_s + m_5\frac{\pi}{2}\right] \right. \\ &\quad \left. - \cos\left[m_1\omega_0 + m_2\Omega_0 + m_3\lambda_n + m_4\Omega_s + m_5\frac{\pi}{2}\right]\right\} \end{aligned} \tag{7}$$

where the set of vectors $\{(m_1, m_2, m_3, m_4, m_5)\}$ specifies the linear combinations of angles found in Eq. (5). The coefficients $C(a_0, e_0, i_0;$ parameters) are functions of the initial mean elements and parameters such as the harmonic coefficients J_{lm} and the third-body orbit elements.

The analytical model defined in Eq. (7) yields a convenient method for ascertaining the behavior of eccentricity over time as a function of initial values. As an example, consider a satellite with $(\Omega, \lambda_n) = (188.089, 19.638$ deg), this represents satellite A4 with a slightly different argument of latitude ($u = 64.638$ deg) or a slightly different defining epoch time ($\theta_e = 197.71$ deg). The initial eccentricity has been set at $e = 0.01$. When these values are used, eccentricity is computed as a function of the initial perigee value and time and is shown in Fig. 6. It is evident from Fig. 6 that most values of perigee below 180 deg yield eccentricities that grow to near 0.015, and above 180 deg, many approach zero. Note that there is a small region where the eccentricity is less than zero; this is an artifact of the perturbation method. One technique to avoid this is to rescale

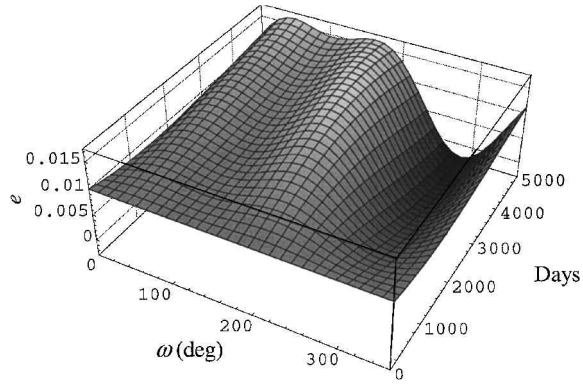

Fig. 6 Analytical eccentricity behavior as a function of initial perigee and time, obtained using standard perturbation theory.

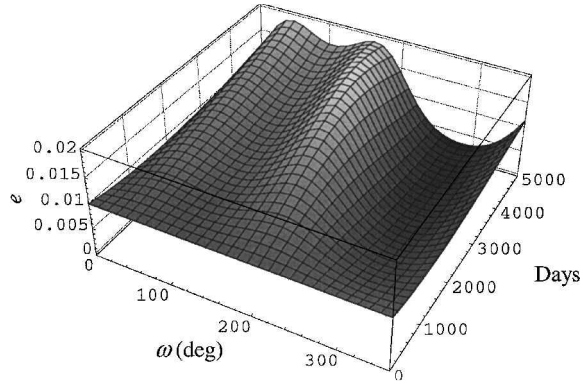

Fig. 7 Analytical eccentricity behavior as a function of initial perigee and time, obtained using nonuniform perturbation result.

Eq. (6) by dividing by e and integrating as before. Doing so yields a function of time for eccentricity that formally has the form

$$e(t) = e_0 \exp\left[\sum \frac{C}{e_0(m_1\dot{\omega} + m_2\dot{\Omega})}\cos(\cdot)\right] \tag{8}$$

This approach was initially utilized for this study, with good results. Indeed, using the same conditions as those utilized to create Fig. 6 and applied to Eq. (8) produces the eccentricity behavior shown in Fig. 7. Now there is no region that yields negative values for eccentricity, and qualitatively the results are very similar to those from the standard theory. However, unlike the standard approach, the result in Eq. (8) has terms of order $\mathcal{O}(J_{22}/e_0)$ because of the coupling with the tesseral harmonics. This result is not asymptotic as $e_0 \to 0$; hence, the predicted behavior diverges from the true behavior. Numerically, if the coupling tesseral terms yield an order of less than $\mathcal{O}(1)$, then Eq. (8) yields satisfactory results as seen in Fig. 7. However, this result is local and nonuniform in e_0. Because Eq. (7) is uniform, it is preferred for assessing the qualitative behavior of eccentricity.

Returning to the example of satellite A4 with the modified nominal node ($\lambda_n = 19.638$ deg), the shift in node coupled with an anticipated growth of eccentricity of $\Delta e = 0.003$ places the satellite trajectory in a region that should encounter an action rate zero (Fig. 2). The controlled trajectory result is shown in Fig. 8. It is evident from the semimajor axis history and the nodal history that the trajectory passes through an action rate zero during the third cycle (1900–3500 days). The EOSK algorithm compensates by redefining target boundaries and performing a maneuver to drift to the new burn boundary (~18 deg). The behavior of eccentricity is shown in the middle plot. The numerically propagated result is shown with the solid line, and the analytically propagated result [using Eq. (7)] is shown with the dashed line. The analytical result correctly captures the qualitative behavior and is quantitatively accurate to within 10% of the true values. Comparisons (not shown) with the other trajectories examined in this study yield similar qualitative and quantitative agreement. When the combination of the action zero locations

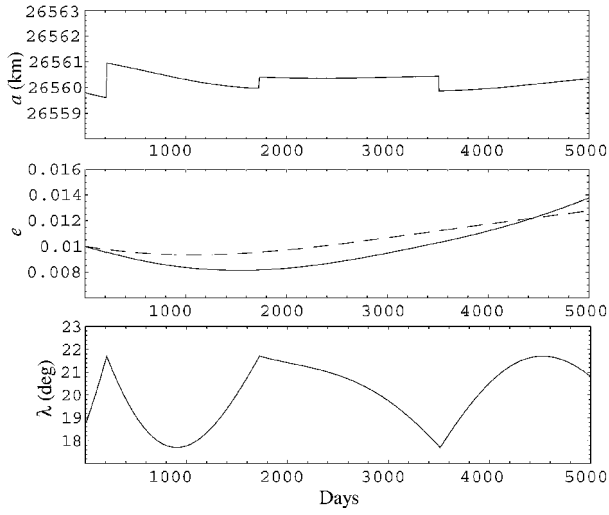

Fig. 8 Figure 3 initial conditions except perigee shifted from an initial value from 0 to 8 deg; action rate zero is encountered, and the EOSK algorithm compensates. Dashed line in the eccentricity figure is analytically predicted value using the standard perturbation theory, Eq. (7).

predicted using Eq. (4a) and the analytical behavior of eccentricity from Eq. (7) is used, it is now possible to ascertain the likelihood that a specific GPS mission will encounter an action rate zero and the need to utilize a robust SK approach, such as the EOSK algorithm.

Conclusions

These results indicate that an orbit with an inclination in the region near 55 deg and with modest eccentricity can encounter significant portions of phase space that have action rate zeros. The location of these zeros is primarily a function of the nominal stroboscopic mean node, perigee, and eccentricity. The curves defining these locations as functions of eccentricity and inclination become increasingly complex with a modest growth in eccentricity. This study has also shown that the combined interaction of luni–solar perturbations and tesseral harmonics (with a stationary stroboscopic mean node) dominates the behavior of eccentricity and can lead to a growth of eccentricity. Indeed, it is possible that eccentricity changes over a mission lifetime can put a satellite orbit that initially avoided action rate zeros into a region of space where it will likely encounter them. This has potentially significant operational impacts. The next phase GPS satellites are to be delivered into their final orbits with eccentricities not to exceed 0.012. The preceding analysis shows that GPS satellites in orbits with borderline eccentricities may run the risk of encountering SK instabilities using traditional techniques. Utilizing an enhanced SK method (such as the EOSK approach), repositioning the satellite to avoid the action rate zeros, or controlling eccentricity are all potential strategies for solving this problem. At a minimum, once an operational orbit is attained, an assessment should be made as to the likelihood of the satellite encountering these instabilities during the mission lifetime.

Appendix: Equations for Secular Rates and Long Period Harmonics

Detailed equations for the secular rates are as follows:

$$\dot{\omega}_{\text{sec}} = \frac{3}{4}\frac{nJ_2}{(1-e^2)^2}(4-5\sin^2 i) + \frac{3}{512}\frac{n_l^2}{n} \times \frac{[8+7e^2+(16+9e^2)\cos 2i]}{(1-e^2)^2}(1+3\cos 2i_l)(1+3\cos 2o_e) + \frac{3}{128}\frac{n_s^2}{n}\frac{[8+7e^2+(16+9e^2)\cos 2i]}{(1-e^2)^2}(1+3\cos 2i_s) \quad \text{(A1)}$$

$$\dot{\Omega}_{\text{sec}} = -\frac{3}{2}\frac{nJ_2}{(1-e^2)^2}\cos i - \frac{3}{128}\frac{n_l^2}{n}\frac{(2+3e^2)\cos i}{(1-e^2)^2}(1+3\cos 2i_l) \times (1+3\cos 2o_e) - \frac{3}{32}\frac{n_s^2}{n}\frac{(2+3e^2)\cos i}{(1-e^2)^2}(1+3\cos 2i_s) \quad \text{(A2)}$$

where n, n_l, and n_s refer to the mean motion rates of the satellite, the moon, and the sun, respectively. The angle o_e is the obliquity of the ecliptic. Recall that all lunar orbit parameters are referenced to the ecliptic plane, and solar apparent orbit parameters are referenced to the Earth's equatorial plane. Detailed equations for the long period harmonic terms identified in the Hamiltonian of Eq. (5) take the form

$$V^l_{\text{GPS}} = e^2\frac{\mu_l}{a_l}\left(\frac{a}{a_l}\right)^2\left(\frac{3}{4}\sin^2 i_l - \frac{1}{2}\right)\left\{\frac{15}{8}\sin^2 i(1+3\cos o_\varepsilon) \times \cos 2\omega - \frac{15}{16}\sin i(1+\cos i)\sin 2o_\varepsilon\cos(2\omega+\Omega)\right\} + \mathcal{O}(e^3) \quad \text{(A3)}$$

$$V^s_{\text{GPS}} = e^2\frac{\mu_s}{a_s}\left(\frac{a}{a_s}\right)^2\left\{\frac{15}{8}\sin^2 i\left(\frac{3}{4}\sin^2 i_s - \frac{1}{2}\right)\cos 2\omega + \frac{15}{16}\sin i(1+\cos i)\sin i_s\cos i_s\cos(2\omega+\Omega-\Omega_s)\right\} + \mathcal{O}(e^3) \quad \text{(A4)}$$

$$V^t_{\text{GPS}} = -\frac{\mu}{a}\left\{\frac{15}{8}\left(\frac{R_e}{a}\right)^3\sin i(1-2\cos i-3\cos^2 i)J_{32} \times \cos[2(\lambda-\lambda_{32})] - \frac{3}{8}e\left(\frac{R_e}{a}\right)^2(1+\cos i)^2 J_{22} \times \cos[2(\lambda-\lambda_{22})+\omega] + \frac{9}{4}e\left(\frac{R_e}{a}\right)^2\sin^2 J_{22} \times \cos[2(\lambda-\lambda_{22})-\omega]\right\} + \mathcal{O}(e^2) \quad \text{(A5)}$$

$$V^z_{\text{GPS}} = -\frac{3}{2}e\frac{\mu}{a}\left(\frac{R_e}{a}\right)^3 J_3\left\{\frac{5}{4}\sin^3 i - \sin i\right\}\cos\left(\frac{\pi}{2}-\omega\right) + \mathcal{O}(e^3) \quad \text{(A6)}$$

Acknowledgments

This research was partially supported by the Jet Propulsion Laboratory, California Institute of Technology, under contract with NASA. The author would like to thank John Cox, George Chao, James Gidney, and Matthew Hart of The Aerospace Corporation for their helpful discussions regarding this work and for providing details regarding the GPS constellation operational requirements and orbit parameters.

References

[1] Ely, T. A., and Howell, K. C., "Long Term Evolution of Artificial Satellite Orbits Due to Resonant Tesseral Harmonics," *Journal of Astronautical Sciences*, Vol. 44, No. 2, 1996, pp. 167–190.

[2] Gedeon, G. S., "Tesseral Resonance Effects on Satellite Orbits," *Celestial Mechanics*, Vol. 1, No. 2, 1969, pp. 167–189.

[3] Kamel, A., Ekman, D., and Tibbitts, R., "East-West Stationkeeping Requirements of Nearly Synchronous Satellites Due to Earth's Triaxiality and Luni-Solar Effects," *Celestial Mechanics*, Vol. 8, No. 1, 1973, pp. 129–148.

[4] Chao, C., and Schmitt, D., "Eliminating GPS Stationkeeping Maneuvers by Changing the Orbit Altitude," American Astronautical Society, AAS Paper 89-407, Aug. 1989.

[5] Ely, T. A., and Howell, K. C., "East-West Stationkeeping of Satellite Orbits with Resonant Tesseral Harmonics," *Acta Astronautica*, Vol. 46, No. 1, 2000, pp. 1–15.

[6] Goldstein, H., *Classical Mechanics*, 2nd ed., Addison Wesley Longman, Reading, MA, 1980, Chap. 10, pp. 463–471.

[7] Ely, T. A., and Howell, K. C., "Dynamics of Artificial Satellite Orbits with Tesseral Resonances Including the Effects of Luni-Solar Perturbations," *International Journal of Dynamics and Stability of Systems*, Vol. 12, No. 4, 1997, pp. 243–269.

[8] Giacaglia, G. E. O., "Third Body Perturbations on Satellites," *Proceedings of the Artificial Satellite Theory Workshop*, U.S. Naval Observatory, 1993, pp. 73–155.